Size Effect on Elastic Stress Concentrations in Unidirectional Fiber Reinforced Soft Composites

Chung-Yuen Hui[1,2*], Zezhou Liu[1] and S. Leigh Phoenix[1]

[1]Sibley School of Mechanical and Aerospace Engineering, Field of Theoretical and Applied Mechanics, Cornell University, Ithaca, NY 14853, USA

[2]Global Station for Soft Matter, GI-CoRE, Hokkaido University, Sapporo, Japan

*Corresponding Author, 322 Thurston Hall, Cornell University, Ithaca, NY 14853, USA. ch45@cornell.edu

Key words: crack; soft composites; equal load-sharing; local load-sharing

Abstract: We revisit the classic problem of determining stress concentrations on neighboring fibers to multiple, transversely-aligned fiber breaks in a planar, unidirectional fiber-matrix composite. Fibers are assumed to be perfectly bonded to the elastic matrix. Finite size effects on stress concentration are studied by varying the overall length of the composite relative to the characteristic load transfer length between broken and intact fibers. As an alternative to the discrete fiber and matrix framework in the classic analysis of Hedgepeth, and its extension by Hikami and Chou, the fiber stress distribution in the composite is obtained through continuum modeling of the composite as a highly anisotropic elastic plate, whereby the stresses and stress concentration factors at fiber locations in the discrete model are extracted in a closed form. For composites of finite length, the stress concentration factors determined using the continuum model compare favorably with numerical solution of the discrete shear-lag model. In the limit of a plate with infinitely long fibers, our stress concentration factors also agree well with the exact results of Hikami and Chou. For composites having a length less than the characteristic elastic load transfer length, and loaded under displacement boundary conditions, we show that local stress concentrations vanish irrespective of the size of the crack or the number of fiber breaks. This behavior becomes important when modeling and interpreting laboratory experiments on the mechanical behavior of recent soft composite specimens consisting of stiff fibers in an extremely compliant elastic matrix.

1. Introduction

A fundamental problem in composite strength theory is the mechanics of load transfer around clusters of fiber breaks that often develop in a unidirectional fiber-matrix composite when loaded. It is well known that the formation of such clusters of broken fibers depends both on the statistically-distributed fiber strength [1–4] and on the mechanism of stress redistribution from broken to intact fibers [5–9]. When a fiber in the composite breaks at a flaw, the two local regions of the fiber on each side of the break unload to zero at the break over some length, and the original loads carried by these segments are transferred laterally onto neighboring intact fibers. This

causes these neighbors to be overloaded, and thus more susceptible to failure near the break. The characteristic length of this overload region, which depends on the mechanical and geometric properties of the fiber and surrounding matrix, is roughly the same as that of the unloaded fiber segments, and is an important length scale in composite strength theory; it is often called the effective load transfer length (when viewed in terms of local fiber overloads), or ineffective length (when viewed in terms of the lost load carrying the broken fiber). This load transfer process has been originally demonstrated using a shear-lag model by Hedgepeth [5], and extensively studied to improve the accuracy and realism under certain circumstances [10,11]. Fiber break evolution in unidirectional composites has also been investigated in detail [12,13]. As failure progresses, and the break cluster size increases, the stress concentrations in the neighboring intact fibers also increase, as does actual length of load transfer on these fibers.

In order to model the failure process and overall statistical strength distribution of large composites, idealized models of the stress redistribution from broken to intact fibers are often used, as well as idealizations of the geometry of the statistical fiber break progression in growing break clusters. Such idealizations are typically necessary to keep computations tractable, especially when seeking to gain analytical insight into the scaling of the strength distribution with composite volume, as well as the behavior of the lower distribution tail important to establishing maximum permissible composite load levels consistent with maintaining high reliability [14]. More elaborate finite element models [15–24] can be very useful for providing benchmark fiber and matrix stress distribution results, but computational demands limit the size scales and numbers of fibers that can be treated. These are often too small to uncover large-scale statistical behavior that ultimately emerges in composite structures used in engineering applications. Also, studies involving more elaborate Monte Carlo simulations [25–29] of the statistical failure process based on more detailed micromechanical models that accommodate the longitudinal staggering of fiber breaks, have repeatedly shown that while the failure patterns in break clusters may appear to be very different from their idealizations, the shapes of the resulting probability distributions for composite strength are affected surprisingly little and in ways amenable to straightforward scaling factors.

Idealized models representing two extremes for the stress redistribution mechanism have been used extensively in the literature, mainly because of their simplicity. At one extreme, are equal load-sharing (ELS) models [30,31] together with their global load-sharing (GLS) generalizations [32,33], and at the other extreme are local load-sharing (LLS) models [5,6,9,34]. In ELS models the fundamental assumption is that, as failure progresses, all failed fibers over a certain bundle length carry no load, and all surviving fibers share the applied load equally. In GLS models the same general principle applies at a cross-sectional plane except that a nearby failed fiber may still carry some load at that plane, as determined by a slip-length around the fiber break over which the fiber gradually unloads. These two models, ELS and GLS are typically applied to composites where the matrix has a low yield strength in shear, and/or readily debonds from the fiber, leaving only weak coupling between fibers. In these cases, the stress redistribution from broken to intact fibers becomes far more diffuse over

many fibers and over much longer lengths, as illustrated for instance in Beyerlein and Phoenix [9] Thus, immediate neighbors see almost no stress concentration compared to others receiving extra load from failed fibers. Consequently, ELS and GLS models cannot predict the formation of growing clusters of breaks; however, they do capture the influence of fiber strength statistics in determining composite strength behavior.

LLS models apply to composites where the matrix is elastic and resistant to yielding and debonding from the fiber, and thus, the load of failed fibers is redistributed mostly onto a few nearby intact neighbors. Consequently, formation of growing fiber break clusters and their ultimate instability resulting in composite failure is a natural feature of LLS models. Within the general LLS framework, many modelling approaches have been developed to calculate realistic stress concentration profiles in fibers next to break clusters. For instance, Hedgepeth and Van Dyke [6] extended the previously mentioned, shear-lag analysis of Hedgepeth [5] to 3D unidirectional composites having fibers arranged in both hexagonal and square arrays. Goree and Gross [35] also extended this 2D model and found an approximate solution for the stress field around certain clusters in a 3D composite containing a square array of linearly elastic fibers in an infinite linearly elastic matrix. However, only numerical values of fiber stress concentrations were determined for certain failure configurations, which did not suggest useful analytical approximations applicable to other configurations. More recently, Mahesh et al. [36,37] were able to determine such analytical approximations in 3D settings, which compared favorably to numerical solutions of the shear-lag model. These were used together with Weibull fiber strength behavior to generate analytical distributions for composite strength based on fiber break cluster growth, which compared favorably to Monte Carlo simulation results of the same failure process but based on numerical solution of the shear-lag equations.

Other researchers have developed models in the spirit of LLS but focusing on additional aspects of practical importance such as effects of number of fibers [38,39], random fiber arrangement and spacing [40], plastic yielding and debonding of the fiber-matrix interface [6,9], mixing of two fiber types which is often referred to as hybrid composites [33,41], and lifetime creep/rupture [42,43] among others. Some build on spring element models [44,45] whose numerical results are fit with analytical functions to extend their utility when calculating fiber failure probabilities in various configurations. Others make use of finite element (FE) calculations to arrive at similar analytical approximations that are incorporated into an influence function approach to model fiber overloads in larger, and more irregular break cluster geometries, e.g. Swolfs et al. [23]. These models are often used in simplified probability calculations of composite failure based on Weibull fiber strength, and others use them in Monte Carlo simulations of the composite failure process under comparable assumptions.

The development of LLS models owes much to the seminal, analytical work of Hedgepeth [5], who provided an exact solution for stress redistribution onto fibers next to a transversely-aligned group of broken fibers in a unidirectional fiber-matrix composite. The composite was in the form of a 2D planar sheet consisting of a parallel array of *infinitely* long fibers perfectly bonded to an elastic matrix separating them, and where the group of broken

fibers was reminiscent of a crack, as shown in Fig. 1. Hedgepeth found an expression for the "peak" stress concentration factor (SCF) $K_{n,1}^{\infty}$ for the first intact fiber next to a cluster of n adjacent breaks, this being

$$K_{n,1}^{\infty}=\frac{(4)(6)\cdots(2n)(2n+2)}{(3)(5)\cdots(2n-1)(2n+1)}=\prod_{j=1}^{n}\frac{(2j+2)}{(2j+1)}. \tag{1a}$$

The superscript '∞' indicates that fibers have infinite length. Hikami and Chou [8] extended this result and obtained an exact expression for $K_{n,s}^{\infty}$ on fiber number s directly ahead of the last broken fiber along the crack plane (see Fig. 1):

$$K_{n,s}^{\infty}=(n+2s-1)\frac{(2s)(2s+2)(2s+4)\cdots(2s+2n-2)}{(2s-1)(2s+1)(2s+3)\cdots(2s+2n-1)}. \tag{1b}$$

Various attempts have been made to find a simpler approximate expression for $K_{n,s}^{\infty}$. For example, Beyerlein et al. [46] used Stirling's formula to derive several approximate expressions for the stress concentration factor given by (1a,b), and Phoenix and Beyerlein [47] found that $K_{n,1}^{\infty}\approx\sqrt{1+\pi n/4}$ with an error less than 0.25 percent.

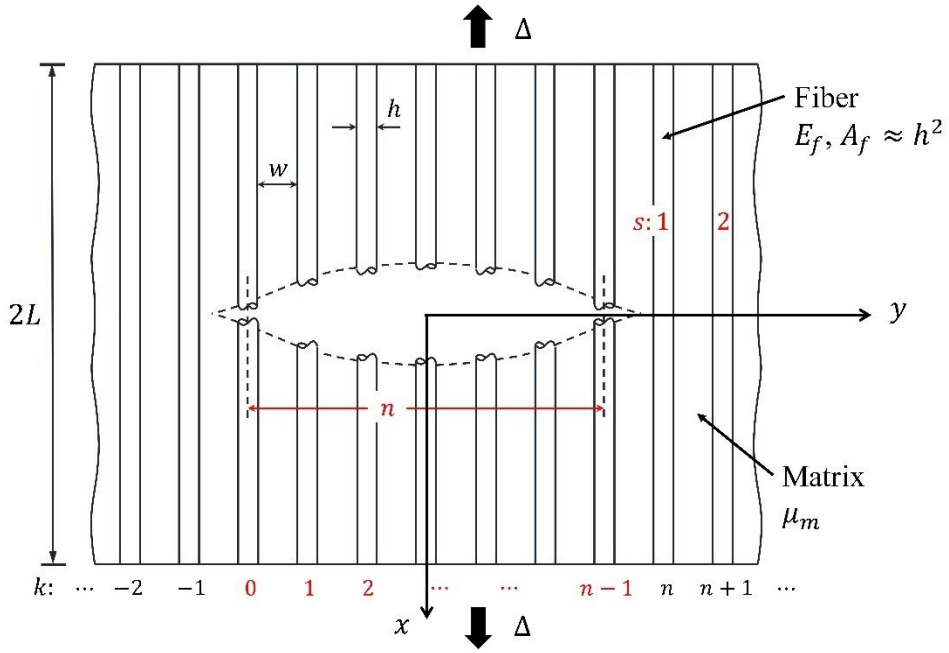

Fig. 1. Planar 2D composite with elastic fibers embedded in an elastic matrix. A group of n consecutive fibers is broken, forming a crack-like structure. x-axis is along the fiber direction, and y-axis is along the transverse direction. The height of the composite is $2L$ (in Hedgepeth $L\to\infty$), and a uniform vertical displacement $\pm\Delta$ is imposed on the upper and lower surface of the composite. Integer k is used to label fibers where $-\infty<k<\infty$, and the n contiguous broken fibers span $0\le k<n-1$. Integer s denotes the s^{th} intact fiber ahead of the last broken fiber along the crack plane, where s = 1 corresponds to the first intact fiber.

However, there are two limitations on these previous works. The first one is that, for equation (1) these approximations work well only when $n >> s$ (except for an approximation found by Phoenix and Beyerlein [47] that is accurate, but only for $s = 1$). We are not aware of any approximation expression that works for the full range of n and s. In this work, we provide such an expression (see eq. (19)). The other limitation is that most of analytical and numerical studies assume the composite length is much larger than the load transfer length, and as a consequence the composite is often taken to be infinitely long in some analytical models [5,8]. This assumption is reasonable for traditional composites in which the ratio of modulus of fiber to matrix is below 100. But it is not the case for the emerging class of soft composites [48–51]. These soft composites consist of traditional stiff fibers embedded in a very soft but tough matrix. Indeed, the matrices in these composites have shear moduli as low as kPa, and can withstand strains up to 1000% [48,49]. It has been found out that these soft composites exhibit extremely high effective toughness, high tear strength, high tensile modulus, and low bending modulus, and have many potential applications, e.g. soft biological prosthetics [52–54]. To illustrate the idea of finite length of soft composites, let us consider the key length scale in the Hedgepeth solution: the load transfer length, l_T. Physically, l_T represents the extent of the overload region along a fiber near a fiber break. In the Hedgepeth theory, this load transfer length is, to within a quantity of order 1,

$$l_T \approx \sqrt{\frac{E_f A_f}{\mu_m}}, \tag{2}$$

where A_f is the cross-sectional area of a fiber, E_f is the Young's modulus of fiber and μ_m is the shear modulus of the matrix. Many tough soft matrices have shear moduli on the order of 0.1 MPa or less. For E-glass fibers used in Huang et al. [49], $E_f \approx 74$ GPa, thus

$$l_T \approx \sqrt{\frac{74\times10^9}{10^5}}\sqrt{A_f} \approx 8.6\times10^2\sqrt{A_f}. \tag{3}$$

Taking the fiber radius to be 7 microns [49], $\sqrt{A_f} \approx 1.2\times10^{-5}$ m, and thus, $l_T \approx 1$ cm. In contrast, if the soft matrix were replaced by an epoxy, then $l_T \approx \sqrt{\frac{74\times10^9}{1.25\times10^9}}\sqrt{A_f} \approx 7.7\sqrt{A_f}$ which is roughly 0.09 mm. Since the size of typical samples are on the order of centimeters, a composite sample with an epoxy matrix can be considered as infinite, which is not true for a composite sample with a soft matrix. This motivates us to study size effects, that is, instead of infinitely long fibers, the length of fibers in our unidirectional composite is finite. In this study, we provide an expression of SCF based on continuum mechanics for more general case where the composite length is finite.

The plan of this paper is as follows. In the methods section, we first summarize the shear-lag model of Hedgepeth [5] and then introduce a continuum model to determine the stress and strain in the composite. In the results section, we present a closed-form solution for the continuum model. We solve the shear-lag model numerically and compare these results with the continuum model. We present an approximate formula for the stress concentration factor for a composite where fibers have finite length, L (in the following this is denoted by $K_{n,s}^{L}$). We also compare $K_{n,s}^{\infty}$ with the exact result of Hikami and Chou [8].

2. Methods

The geometry is shown in Fig. 1. The composite consists of a 2D array of parallel fibers of length 2L and Young's modulus E_f. The fibers are perfectly bonded to an elastic matrix of shear modulus μ_m. The composite is infinite in the y direction and has n consecutive fiber breaks along the center line $x = 0$. A uniform vertical displacement $\pm\Delta$ is imposed on the upper and lower surface of the composite plate at $x = \pm L$, thus the strain far away from the crack is $\varepsilon = \Delta / L$. All fibers have the same cross-sectional area A_f. The effective matrix width between fibers is w and the effective fiber size is h. As in Phoenix and Beyerlein [47] we focus on the main mechanical effects, and not concerned ourselves with the cross-sectional geometry of the fibers (e.g., round or square).

2.1 Discrete Model

We briefly summarize the shear-lag model of Hedgepeth [5]. Details can be found in Hedgepeth [5] and Hikami and Chou [8]. The key idea is that fibers can support only tension and the matrix can only carry shear. As shown in Fig. 1, we use an integer k to label fibers, for example, $u_k(x)$ and $p_k(x)$ denote the displacement and load of the k^{th} fiber. Following Hedgepeth, we introduce the load transfer length

$$l_T \equiv \sqrt{\frac{E_f A_f w}{\mu_m h}}. \tag{4}$$

We introduce the normalization for position along a fiber, load and displacement

$$\xi = x / l_T,\ P_k = \frac{p_k}{E_f A_f \varepsilon},\ U_k = \frac{u_k}{\varepsilon l_T},\quad \varepsilon = \Delta / L. \tag{5}$$

The governing equations is a system of ODEs and were given by Hedgepeth [5] as

$$\frac{\partial^2 U_k}{\partial \xi^2} + U_{k+1} - 2U_k + U_{k-1} = 0,\quad k = \cdots, -3, -2, -1, 0, 1, 2, 3, \cdots \tag{6}$$

The boundary conditions of the finite fiber length problem are:

$$U_k(0)=0 \quad (k<0,\ k\geq n), \qquad \frac{dU_k}{d\xi}(0)=0 \quad (0\leq k\leq n-1), \qquad U_k(L/l_T)=L/l_T \tag{7}$$

The first condition is the symmetry condition where all unbroken fibers have zero displacement on the mid-plane. The second condition states that the force on the broken fiber end is zero. The last condition is the applied displacement boundary condition. Numerical solution of this discrete model, equations (6) and (7), can be easily obtained by any boundary value problem (BVP) solvers (e.g., bvp4c in Matlab, or solve_bvp in Python), and it will be used to compare with the solution of the continuum model below.

2.2 Continuum model

We seek an approximate solution using a continuum description where the composite is modeled as a highly anisotropic plate [46,55]. As noted by Hedgepeth [5] and Hedgepeth and Van Dyke [6], equation (6) is a discrete version of the Laplace equation. Our approach is similar but simpler than the model proposed by Beyerlein et al. [46] who model the composite as an orthotropic medium. More details of the continuum model described below can be found in Sha et al. [55] which use the same approach to study the stress state near a crack tip inside a craze. Note, in fracture mechanics the convention is that x_1-axis is along the crack plane direction, and x_2-axis is perpendicular to the crack. Connected with the discrete model by Hedgepeth, x_1-axis in our continuum model corresponds to y-axis in Fig. 1 (transverse direction), and x_2-axis corresponds to x-axis (fiber direction). Accordingly, the normal stress σ_{xx} in the fibers and shear stress σ_{xy} in the matrix correspond to σ_{22} and σ_{12} in our continuum model, respectively. The unidirectional composite in Fig. 1 is modeled as a plane stress orthotropic solid with

$$\begin{aligned}
\sigma_{11} &= \sigma_{yy} = C_{11}\varepsilon_{11} + C_{12}\varepsilon_{22} + C_{13}\varepsilon_{33} \\
\sigma_{22} &= \sigma_{xx} = C_{12}\varepsilon_{11} + C_{22}\varepsilon_{22} + C_{23}\varepsilon_{33}\ , \\
\sigma_{12} &= \sigma_{xy} = 2C_{66}\varepsilon_{12}
\end{aligned} \tag{8a-c}$$

where ε_{ij} are the strains, and C_{ij} are the standard moduli for an orthotropic plate. In particular, assuming $E_f >> \mu_m$ and using the rule of mixtures [46],

$$C_{12} \approx \frac{\mu_m}{1-V_f}, \text{ and } C_{22} \approx V_f E_f, \tag{8d}$$

where V_f is the volume fraction of fiber. For stiff fibers and compliant matrices, $C_{11} << C_{22}$, $C_{13} << C_{22}$, $C_{23} << C_{22}$ and $C_{12} \approx C_{66} << C_{22}$. Thus, a good approximation for our geometry is to neglect σ_{11} [55] with

$$\sigma_{22} = C_{22}\varepsilon_{22} = C_{22}\frac{\partial u_2}{\partial x_2}$$
$$\sigma_{12} = 2C_{12}\varepsilon_{12} = C_{12}\frac{\partial u_2}{\partial x_1}, \tag{9a,b}$$

where u_2 is the displacement in the vertical or fiber direction. The relevant equilibrium equation is

$$\frac{\partial \sigma_{12}}{\partial x_1} + \frac{\partial \sigma_{22}}{\partial x_2} = 0. \tag{10}$$

Substituting (9a,b) into (10) gives

$$C_{12}\frac{\partial^2 u_2}{\partial x_1^2} + C_{22}\frac{\partial^2 u_2}{\partial x_2^2} = 0. \tag{11}$$

In the continuum model, the 2D planar composite is replaced by an infinitely long elastic strip with height $2L$ (see Fig. 2). The n fiber breaks in the original problem appears as a crack of length a occupying the interval $(-a,0)$ on the x_1-axis. The boundary conditions are

$$\frac{\partial u_2}{\partial x_2}\left(x_1, x_2 = 0^{\pm}\right) = 0 \quad x_1 \in (-a,0), \tag{12a}$$

$$u_2\left(x_1, x_2 = \pm L\right) = \pm\Delta \quad |x_1| < \infty. \tag{12b}$$

Equation (12a) states that the crack formed by the fiber breaks is traction free whereas equation (12b) enforces the displacement imposed on the top and bottom of the composite.

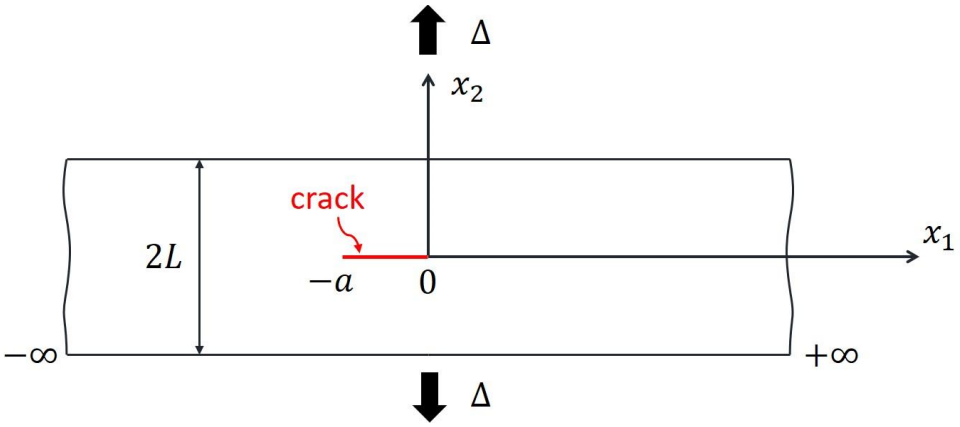

Fig. 2. Geometry of the continuum model, the crack has length a and the infinitely strip has height $2L$. A uniform displacement is imposed on the upper and lower surface.

3. Results

The exact solution of the continuum problem (11) with (12a,b) can be obtained by a transformation of variables and conformal mapping. Due to the finite length of fibers, the discrete problem cannot be solved analytically, however, its solution is obtained numerically by solving a system of ODEs. Here we state the main results. For the continuum problem we define a dimensionless constant

$$\alpha = \sqrt{\frac{C_{22}}{C_{12}}} >> 1 . \tag{13}$$

The stresses σ_{22} and σ_{12} for the continuum model can be written in complex form (see the Appendix), i.e.,

$$\tau(z) \equiv \sigma_{22} + i\sigma_{12} = \frac{C_{22}\Delta\left[\exp\left(\pi z/\bar{L}\right) - \sqrt{\exp\left(-\pi a/\bar{L}\right)}\right]}{L\sqrt{\left(\exp\left(\pi z/\bar{L}\right)-1\right)\left(\exp\left(\pi z/\bar{L}\right) - \exp\left(-\pi a/\bar{L}\right)\right)}}, \tag{14}$$

where $z = x_1 + i\left(x_2/\alpha\right)$ and $\bar{L} = L/\alpha$. In particular, directly ahead of the crack tip, we have $\sigma_{12} = 0$ and

$$\sigma_{22}\left(x_1 > 0, x_2 = 0\right) = \frac{C_{22}\Delta\left[\exp\left(\pi\alpha x_1/L\right) - \sqrt{\exp\left(-\pi\alpha a/L\right)}\right]}{L\sqrt{\left(\exp\left(\pi\alpha x_1/L\right)-1\right)\left(\exp\left(\pi\alpha x_1/L\right) - \exp\left(-\pi\alpha a/L\right)\right)}} . \tag{15a}$$

The factor $\alpha x_1 / L$ in equation (15a) can be written as:

$$\frac{\alpha x_1}{L} = \sqrt{\frac{C_{22}}{C_{12}}}\frac{x_1}{L} = \sqrt{\frac{\left(1-V_f\right)V_f E_f}{\mu_m}}\frac{x_1}{L} = V_f\sqrt{\frac{\left(1-V_f\right)h^2 E_f}{\mu_m V_f}}\frac{x_1}{h}\frac{1}{L} = V_f\frac{x_1}{h}\frac{l_T}{L} = \frac{x_1}{h+w}\frac{l_T}{L} . \tag{15b}$$

The stresses given by the continuum crack solution (14) and (15) have a square root singularity as one approaches the crack tip. Since the continuum solution does not account for the discrete geometry, the position of the crack tip must be interpreted carefully. The position of the crack tip in the continuum model is determined empirically by matching the stress concentration factors of fibers directly ahead of crack tip with the analytic solution of the discrete model by Hikami and Chou [8], which is given by equation (1b). In a previous study, Beyerlein et al. [46] found that the best agreement between the continuum and discrete models occurs when the crack tip is placed at the distance of (h+w)/3 to the left of the first intact fiber. They obtained this result by placing the crack tip at different locations, specifically, at (h+w)/2, 2(h+w)/7, 4(h+w)/17 to the left of the first intact fiber and looking for the best match. Since we use a slightly different and simpler continuum model, we check whether (h+w)/3 is still the "best" position. To do this we place the crack tip at five different locations (i.e., (h+w)/4, (h+w)/3, (h+w)/2, 2(h+w)/3, and 3(h+w)/4 to the left of the first intact fiber) to find the best match and our result turns out to be the same as Beyerlein et al. [46]. Let x_1 be the distance of the s intact fiber from the crack tip, that is

$$\frac{x_1}{h+w} = s - \frac{2}{3}, \quad s \geq 1 . \tag{16}$$

The length of the crack a is

$$\frac{a}{h+w} = (n-1) + 2\times\frac{2}{3} = n+\frac{1}{3}. \tag{17}$$

Using (15a,b) and (16), the SCF $K^L_{n,s}$ is

$$K^L_{n,s} = \frac{\exp\left(\frac{\pi}{\bar{l}}\left(s-\frac{2}{3}\right)\right) - \sqrt{\exp\left(-\frac{\pi}{\bar{l}}\left(n+\frac{1}{3}\right)\right)}}{\sqrt{\left(\exp\left(\frac{\pi}{\bar{l}}\left(s-\frac{2}{3}\right)\right)-1\right)\left(\exp\left(\frac{\pi}{\bar{l}}\left(s-\frac{2}{3}\right)\right)-\exp\left(-\frac{\pi}{\bar{l}}\left(n+\frac{1}{3}\right)\right)\right)}}, \text{ where } \bar{l} = L/l_1. \tag{18}$$

In the limit of an infinite large plate, $\bar{l}\to\infty$, the SCF reduces to

$$K^\infty_{n,s} = \frac{s+\frac{n-1}{2}}{\sqrt{\left(s-\frac{2}{3}\right)\left(s+n-\frac{1}{3}\right)}}. \tag{19}$$

Fig. 3 compares the exact solution of Hikami and Chou [8] given by (1) with (19) for n = 1,2,3,4 and different values of s. Fig. 4 compares the $K^L_{n,s}$ (discrete versus continuum) for n = 1,2,3,4 with different normalized fiber length or composite height. The cross symbols are the analytical solution given by (18) and the circles are numerical results obtained by solving the discrete model (DM). Both figures show that our continuum model can accurately predict the stress concentration factor.

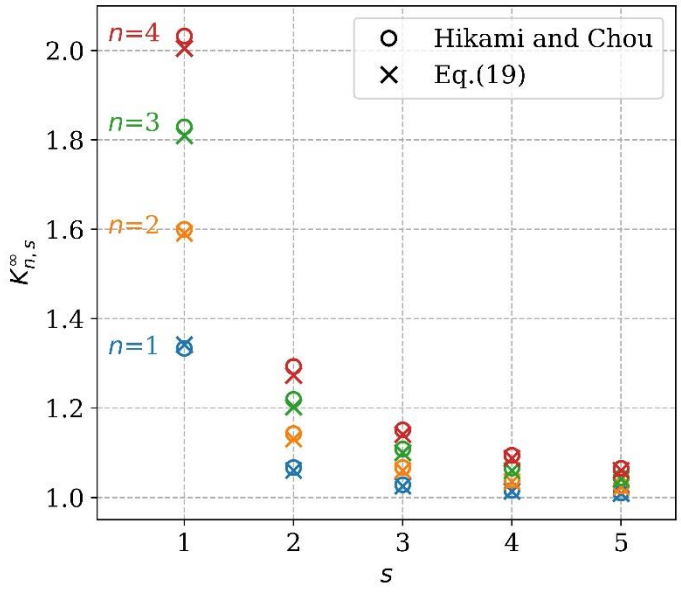

Fig. 3. Comparison of $K^\infty_{n,s}$ by Hikami and Chou, and equation (19), with different values of n and s. The analytic solutions of Hikami and Chou are plotted as circles, and results by equation (19) are plotted as cross symbols.

We point out an interesting result: the stress concentration factor $K^{\infty}_{n,s}$ for an infinite large plate is *independent* of fiber size, matrix spacing and material properties. However, this is not the case when fibers have finite length. Recall in soft composites, the load transfer length l_T can be very large (centimeters), hence fiber length in a small specimen can be less than the load transfer length. This bring up another point. Fig. 4 shows that for short composites, that is, if $\bar{l} = L / l_T << 1$, *all the unbroken fibers are under ELS, that is, all intact fibers bear the same load, irrespectively of the size of the crack.*

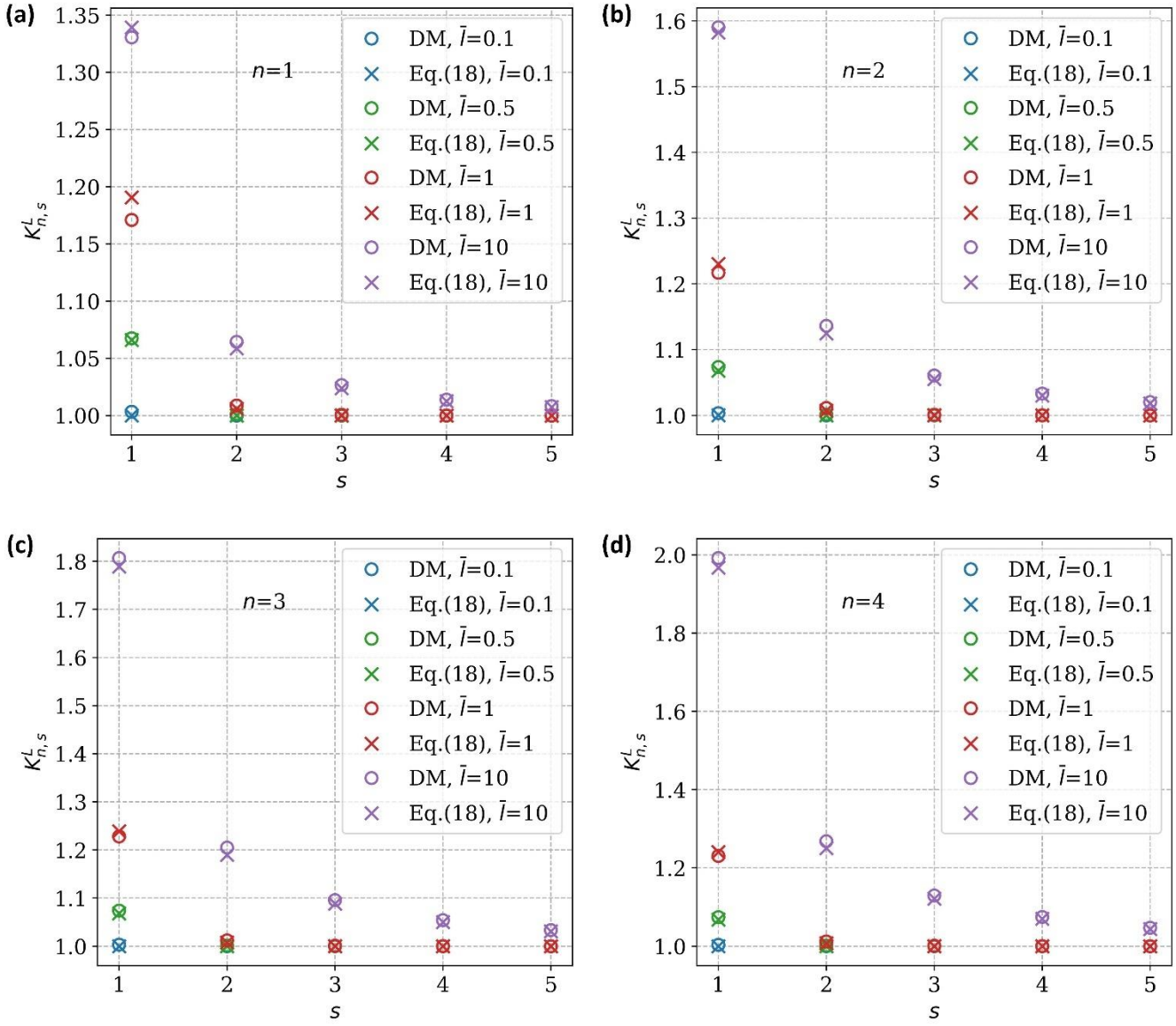

Fig. 4. $K^L_{n,s}$ in the intact fiber s with different normalized length $\bar{l}$. The solutions by discrete model (DM) and equation (18) are plotted as circles and crosses, respectively. (a) $n=1$; (b) $n=2$; (c) $n=3$; (d) $n=4$.

To pursue this idea further, we replace the finite crack in Fig. 2 with a *semi-infinite* crack. The exact stress distribution for this case is obtained by setting $a=\infty$ in equation (14), resulting in:

$$\sigma_{22}\left(x_1,x_2\right)=\frac{C_{22}\Delta}{L}\,\mathrm{Re}\left[\sqrt{\frac{\exp\left(\pi\alpha\left(x_1+ix_2/\alpha\right)/L\right)}{\exp\left(\pi\alpha\left(x_1+ix_2/\alpha\right)/L\right)-1}}\right]$$
$$\sigma_{12}\left(x_1,x_2\right)=\alpha\frac{C_{12}\Delta}{L}\,\mathrm{Im}\left[\sqrt{\frac{\exp\left(\pi\alpha\left(x_1+ix_2/\alpha\right)/L\right)}{\exp\left(\pi\alpha\left(x_1+ix_2/\alpha\right)/L\right)-1}}\right] \tag{20a,b}$$

Using (16) and (20a) with $x_2=0$, the stress acting on the fiber *s* directly ahead of the crack tip is:

$$K^{L}_{\infty,s}=\sqrt{\frac{1}{1-\exp\left(-\pi(s-2/3)/\bar{l}\right)}} \tag{21}$$

Note for $\bar{l}=L/l_T=1/3$ (short composite), the exponential factor in (21) is $\exp\left(-\pi\right)$ for the 1st intact fiber ahead of the crack tip, for the 2nd intact fiber *s* = 2, this factor decreases to $\exp\left(-4\pi\right)$. Accordingly, the SCFs are 1.022 and 1.000, respectively. Hence, in short composites, the intact fibers are under ELS, *irrespective of crack size*. In this regime, the composite is extremely *flaw insensitive despite LLS.*

As a further test of the continuum model, we plot the stress profile along the first intact fiber ($s=1$) for different composite size L and broken fiber number *n*. We use equation (14) to compute the normalized tension $\bar{\sigma}_{22}$ along the fiber, i.e.,

$$\bar{\sigma}_{22}\equiv\frac{\sigma_{22}}{C_{22}\Delta/L}=\mathrm{Re}\left\{\frac{\left[\exp\left(\frac{\pi}{3\bar{l}}\right)\exp\left(i\frac{\pi\bar{x}_2}{3\bar{l}}\right)-\sqrt{\exp\left(-\frac{\pi}{\bar{l}}\left(n+\frac{1}{3}\right)\right)}\right]}{\sqrt{\left(\exp\left(\frac{\pi}{3\bar{l}}\right)\exp\left(i\frac{\pi\bar{x}_2}{3\bar{l}}\right)-1\right)\left(\exp\left(\frac{\pi}{3\bar{l}}\right)\exp\left(i\frac{\pi\bar{x}_2}{3\bar{l}}\right)-\sqrt{\exp\left(-\frac{\pi}{\bar{l}}\left(n+\frac{1}{3}\right)\right)}\right)}}\right\} \tag{22}$$

where $\bar{x}_2=x_2/l_T$. In Fig. 5, we plot the normalized stress $\bar{\sigma}_{22}$ versus the relative position $\bar{x}_2/\bar{l}=x_2/L$ along the fiber with different values of *n* and $\bar{l}$. As shown below, the DM results (symbols) agree with the approximation of equation (22) (lines) within 5% error, irrespective of the value of $\bar{l}$. As expected, for $\bar{l}>>1$, the stress decays very fast within the load transfer length l_T and approaches one; while for the $\bar{l}<<1$, the stress decays very slowly and remains close to one.

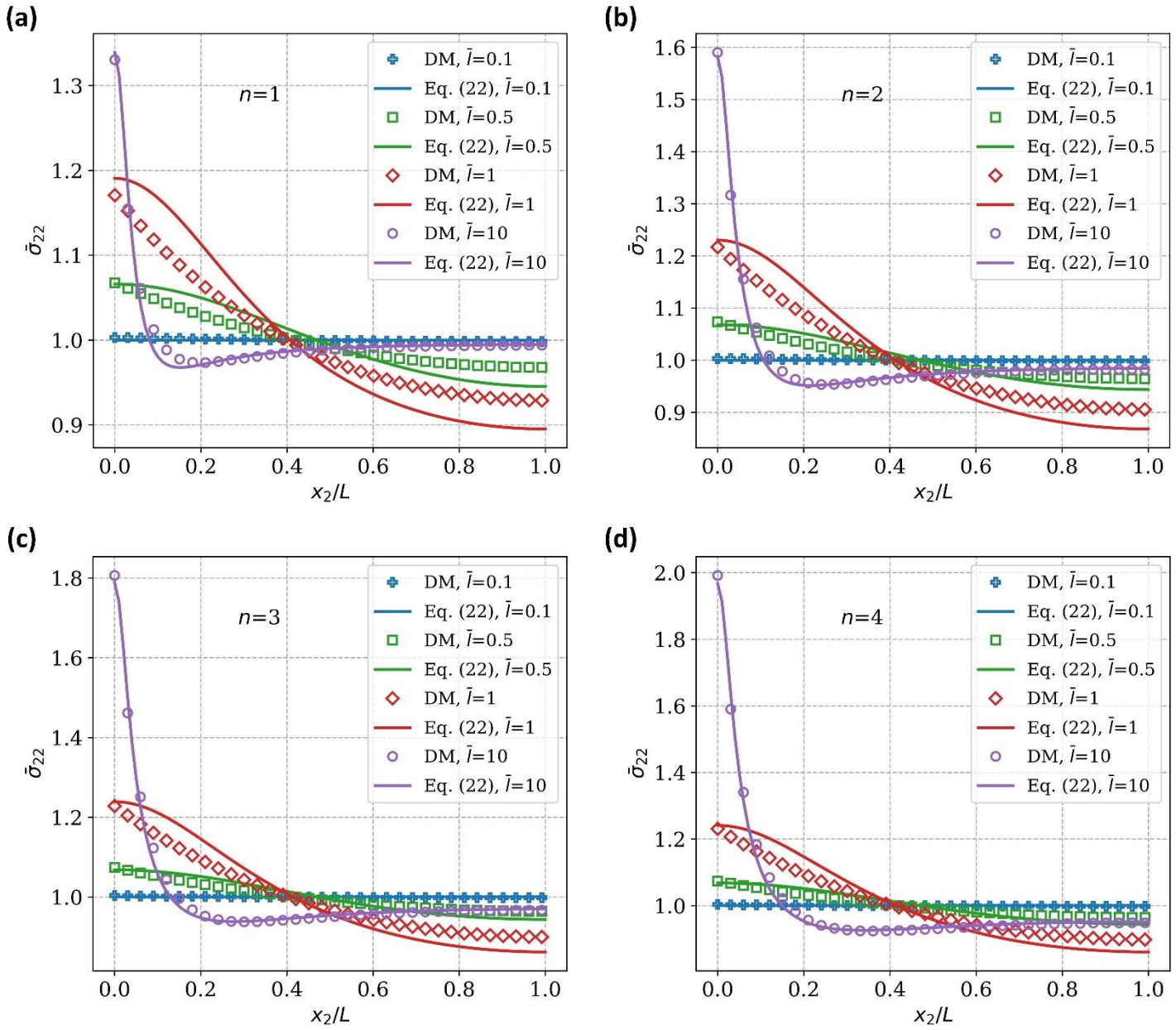

Fig. 5. Normalized stress $\bar{\sigma}_{22}$ versus the relative position x_2 / L along the first intact fiber with different values of n. The solutions by discrete model (DM) and equation (22) are plotted as symbols and lines, respectively. (a) $n = 1$; (b) $n = 2$; (c) $n = 3$; (d) $n = 4$.

4. Summary and Discussion

A continuum model is used to determine the stress concentration factor in a unidirectional fiber-matrix composite with finite length fibers. The stress concentration factor determined using the continuum model compares well with numerical solution of the shear-lag model. It is commonly accepted that a unidirectional composite with elastic matrix is under LLS. Our analysis shows that this is not the case for soft composites where the fiber/matrix modulus ratio is exceedingly large. For this class of composites, small samples are flaw insensitive and ELS is the norm rather than the exception.

For soft composites, this result means that failure of small specimens is governed by ELS and hence by its fiber statistics. Daniels [30] has shown that the failure strength of an ELS bundle consisting of a large number of fibers of equal length δ is asymptotically normally distributed. Specifically, the probability $P(\sigma)$ that the composite fails for nominal stress less than or equal to σ is

$$P(\sigma)=\Phi\left(\frac{\sigma-\bar{\sigma}_{\max}}{\gamma^*}\right),\qquad \Phi(z)=\frac{1}{\sqrt{2\pi}}\int_{-\infty}^{z}e^{-r^2/2}dr \tag{23a,b}$$

where $\bar{\sigma}_{\max}$ is the mean strength and γ^* is the standard deviation. In general, $\bar{\sigma}_{\max}$ and γ^* depend on the fiber strength statistics, and bundle size. A well accepted model is that fibers obey Weibull distribution, that is, the probability that a fiber of length δ will break when subjected to a tensile stress less than or equal to σ is

$$F(\sigma,\delta)=1-\exp\left[-\frac{\delta}{l_0}\left(\frac{\sigma}{\sigma_0}\right)^{\rho}\right]=1-\exp\left[-\left(\frac{\sigma}{\sigma_\delta}\right)^{\rho}\right] \tag{24}$$

where σ_0 is the reference stress associated with a reference length l_0, $\rho>0$ is the Weibull shape parameter, and $\sigma_\delta=(l_0/\delta)^{1/\rho}$. For most fibers, $3<\rho<12$. The smaller the value of ρ, the higher the variability of fiber strength. Using this model, Coleman [56] showed that

$$\bar{\sigma}_{\max}=\sigma_\delta\rho^{-1/\rho}e^{-1/\rho}\quad , \tag{25a}$$

and the standard deviation

$$\gamma^*=\frac{\sigma_\delta}{\sqrt{N}}\rho^{-1/\rho}\sqrt{e^{-1/\rho}\left(1-e^{-1/\rho}\right)}\quad , \tag{25b}$$

where N is the number of fibers in the bundle or composite. In our case, the fiber length is $2L$, $\delta=2L$. Under ELS, we can predict the mean strength and work of extension assuming fibers obey Weibull statistics, and show such composites exhibit the Mullin effect typically observed in rubbers [57] and double network gels [58,59]. This work will be reported in a separated paper.

Our result indicates that linear elastic fracture mechanics (LEFM) breaks down completely for small specimens where ELS prevails. For LEFM to be useful, it is necessary that $L/l_T>>1$ (see equations (15a,b)), that is, fibers in the composite must be much longer than the load transfer length . If this condition is satisfied, then the fiber stress near the crack tip, given by equation (15a), approaches

$$\sigma_{22}(x_1>0,x_2=0)\approx\frac{C_{22}\varepsilon}{\sqrt{(\pi\alpha x_1/L)}}\sqrt{\frac{1-\exp(-\pi\alpha a/2L)}{1+\exp(-\pi\alpha a/2L)}},\quad \pi\alpha x_1/L<<1,\quad x_1\geq(h+w)/3 \tag{26}$$

which has the inverse square root singularity of LEFM if x_1 is allowed to go to zero. For this case, $C_{22}\varepsilon\sqrt{2L/\alpha}\sqrt{\frac{1-\exp(-\pi\alpha a/2L)}{1+\exp(-\pi\alpha a/2L)}}$ corresponds to the stress intensity factor of the crack.

The above analysis is for a 2D planar sheet with equally spaced fibers perfectly bonded to an elastic matrix. It is possible to extend the present analysis to study different fiber packings in 2D using the 3D shear-lag model developed by Hedgepeth and Van Dyke [6]. Mahesh et al. [36] have studied the stress decay along fibers ahead of a penny shaped crack and found similar behavior seen in 2D. Hence we do not expect significant differences in scaling behavior. The analysis in this work is based on linear elasticity where the strains are assumed to be small. However, soft composites can stretch up to 1000% strain, so it may seem that our analysis is impractical. Our analysis can be justified by the fact that, in a displacement-controlled test, a composite sample will reach a peak stress at strains *~0.05 to 0.1* (see for example, Fig. 3C in King et al. [48]). In this regime, linear elasticity is valid. This peak stress is an important mechanical parameter since it characterizes the maximum load capability of the composite. The existence of peak stress is due to competition between stress lost due to fiber breaking and stress gain due to loading. Indeed, as long as fibers can support load, the composite modulus will be significantly larger than matrix modulus and small strain theory is valid. The strain will be large once fibers are highly fragmented. After this point the linear theory break down and there will be a rapid load drop in the stress-strain curve. The analysis in this work allow us to understand the mechanics of load transfer before and during the stress drop. We note that the soft composite in King et al. [48] is a plane weave fabric which has much more complicated micro-mechanics than the unidirectional composite in this study. To study the stress concentrations in such plane weave fabric, one might seek wisdom from the existing analytic models [60,61], and then include the fiber size effect. Here we highlight the differences and connections of soft composites with existing composite theories and LEFM. We hope this work can stimulate interest in soft composites.

Acknowledgments: CYH is supported by National Science Foundation, USA MoMS program under grant number 1903308. SLP acknowledges financial support from National Institute of Standards and Technology, USA under agreement ID 70NANB14H323. This research is motivated by a recent visit of CYH to Jian Ping Gong's laboratory. CYH appreciates discussions with Jian Ping Gong, Daniel King and Wei Cui. We are grateful to the reviewers for their helpful comments.

Conflicts of interest

There are no conflicts to declare.

References

[1] I.J. Beyerlein, S.L. Phoenix, Statistics for the strength and size effects of microcomposites with four carbon fibers in epoxy resin, Composites Science and Technology. 56 (1996) 75–92. doi:10.1016/0266-3538(95)00131-X.
[2] W.A. Curtin, Stochastic Damage Evolution and Failure in Fiber-Reinforced Composites, in: E. van der Giessen, T.Y. Wu (Eds.), Advances in Applied Mechanics, Elsevier, 1998: pp. 163–253. doi:10.1016/S0065-2156(08)70186-8.
[3] F. Tanaka, T. Okabe, H. Okuda, I.A. Kinloch, R.J. Young, Factors controlling the strength of carbon fibres in tension, Composites Part A: Applied Science and Manufacturing. 57 (2014) 88–94. doi:10.1016/j.compositesa.2013.11.007.
[4] Y. Swolfs, I. Verpoest, L. Gorbatikh, Issues in strength models for unidirectional fibre-reinforced composites related to Weibull distributions, fibre packings and boundary effects, Composites Science and Technology. 114 (2015) 42–49. doi:10.1016/j.compscitech.2015.04.002.
[5] J.M. Hedgepeth, Stress concentrations in filamentary structures, NASA TN D-882. (1961).
[6] J.M. Hedgepeth, P. Van Dyke, Local Stress Concentrations in Imperfect Filamentary Composite Materials, Journal of Composite Materials. 1 (1967) 294–309. doi:10.1177/002199836700100305.
[7] J.N. Rossettos, M. Shishesaz, Stress Concentration in Fiber Composite Sheets Including Matrix Extension, J. Appl. Mech. 54 (1987) 723. doi:10.1115/1.3173096.
[8] F. Hikami, T.-W. Chou, Explicit crack problem solutions of unidirectional composites - Elastic stress concentrations, AIAA Journal. 28 (1990) 499–505. doi:10.2514/3.10420.
[9] I.J. Beyerlein, S.L. Phoenix, Stress concentrations around multiple fiber breaks in an elastic matrix with local yielding or debonding using quadratic influence superposition, Journal of the Mechanics and Physics of Solids. 44 (1996) 1997–2039. doi:10.1016/S0022-5096(96)00068-3.
[10] J.A. Nairn, Fracture Mechanics of Unidirectional Composites Using the Shear-Lag Model I: Theory, Journal of Composite Materials. 22 (1988) 561–588. doi:10.1177/002199838802200604.
[11] J.A. Nairn, On the use of shear-lag methods for analysis of stress transfer in unidirectional composites, Mechanics of Materials. 26 (1997) 63–80. doi:10.1016/S0167-6636(97)00023-9.
[12] A. Thionnet, H.Y. Chou, A. Bunsell, Fibre break processes in unidirectional composites, Composites Part A: Applied Science and Manufacturing. 65 (2014) 148–160. doi:10.1016/j.compositesa.2014.06.009.
[13] E.D. McCarthy, J.H. Kim, N.A. Heckert, S.D. Leigh, J.W. Gilman, G.A. Holmes, The fiber break evolution process in a 2-D epoxy/glass multi-fiber array, Composites Science and Technology. 121 (2015) 73–81. doi:10.1016/j.compscitech.2014.10.013.
[14] M. Salviato, Z.P. Bažant, The asymptotic stochastic strength of bundles of elements exhibiting general stress–strain laws, Probabilistic Engineering Mechanics. 36 (2014) 1–7. doi:10.1016/j.probengmech.2014.01.001.
[15] M.R. Nedele, M.R. Wisnom, Three-dimensional finite element analysis of the stress concentration at a single fibre break, Composites Science and Technology. 51 (1994) 517–524. doi:10.1016/0266-3538(94)90084-1.
[16] B. Fiedler, A. Klisch, K. Schulte, Stress concentrations in multiple fibre model composites, Composites Part A: Applied Science and Manufacturing. 29 (1998) 1013–1019. doi:10.1016/S1359-835X(98)00014-1.
[17] P.W.J. van den Heuvel, M.K. Wubbolts, R.J. Young, T. Peijs, Failure phenomena in two-dimensional multi-fibre model composites: 5. A finite element study, Composites Part A: Applied Science and Manufacturing. 29 (1998) 1121–1135. doi:10.1016/S1359-835X(98)00089-X.
[18] K. Goda, The role of interfacial debonding in increasing the strength and reliability of unidirectional fibrous composites, Composites Science and Technology. 59 (1999) 1871–1879. doi:10.1016/S0266-3538(99)00046-9.
[19] C.M. Landis, R.M. McMeeking, Stress concentrations in composites with interface sliding, matrix stiffness and uneven fiber spacing using shear lag theory, International Journal of Solids and Structures. 36 (1999) 4333–4361. doi:10.1016/S0020-7683(98)00193-0.
[20] Z. Xia, T. Okabe, W.A. Curtin, Shear-lag versus finite element models for stress transfer in fiber-reinforced composites, Composites Science and Technology. 62 (2002) 1141–1149. doi:10.1016/S0266-3538(02)00072-6.

[21] S. Blassiau, A. Thionnet, A.R. Bunsell, Micromechanisms of load transfer in a unidirectional carbon fibre–reinforced epoxy composite due to fibre failures. Part 1: Micromechanisms and 3D analysis of load transfer: The elastic case, Composite Structures. 74 (2006) 303–318. doi:10.1016/j.compstruct.2005.04.013.
[22] S. Blassiau, A. Thionnet, A.R. Bunsell, Three-dimensional analysis of load transfer micro-mechanisms in fibre/matrix composites, Composites Science and Technology. 69 (2009) 33–39. doi:10.1016/j.compscitech.2007.10.041.
[23] Y. Swolfs, R.M. McMeeking, I. Verpoest, L. Gorbatikh, Matrix cracks around fibre breaks and their effect on stress redistribution and failure development in unidirectional composites, Composites Science and Technology. 108 (2015) 16–22. doi:10.1016/j.compscitech.2015.01.002.
[24] L. St-Pierre, N.J. Martorell, S.T. Pinho, Stress redistribution around clusters of broken fibres in a composite, Composite Structures. 168 (2017) 226–233. doi:10.1016/j.compstruct.2017.01.084.
[25] K. Goda, S.L. Phoenix, Reliability approach to the tensile strength of unidirectional CFRP composites by Monte-Carlo simulation in a shear-lag model, Composites Science and Technology. 50 (1994) 457–468. doi:10.1016/0266-3538(94)90054-X.
[26] I.J. Beyerlein, S.L. Phoenix, Statistics of fracture for an elastic notched composite lamina containing Weibull fibers— Part I. Features from Monte-Carlo simulation, Engineering Fracture Mechanics. 57 (1997) 241–265. doi:10.1016/S0013-7944(97)00012-X.
[27] I.J. Beyerlein, S.L. Phoenix, Statistics of fracture for an elastic notched composite lamina containing weibull fibers—Part II. Probability models of crack growth, Engineering Fracture Mechanics. 57 (1997) 267–299. doi:10.1016/S0013-7944(97)00013-1.
[28] C.M. Landis, I.J. Beyerlein, R.M. McMeeking, Micromechanical simulation of the failure of fiber reinforced composites, Journal of the Mechanics and Physics of Solids. 48 (2000) 621–648. doi:10.1016/S0022-5096(99)00051-4.
[29] A. Gupta, S. Mahesh, S.M. Keralavarma, Strength distribution of large unidirectional composite patches with realistic load sharing, Phys. Rev. E. 96 (2017) 043002. doi:10.1103/PhysRevE.96.043002.
[30] H.E. Daniels, The statistical theory of the strength of bundles of threads. I, Proceedings of the Royal Society of London. Series A. Mathematical and Physical Sciences. 183 (1945) 405–435. doi:10.1098/rspa.1945.0011.
[31] B.W. Rosen, Tensile failure of fibrous composites, AIAA Journal. 2 (1964) 1985–1991. doi:10.2514/3.2699.
[32] W.A. Curtin, Theory of Mechanical Properties of Ceramic-Matrix Composites, J American Ceramic Society. 74 (1991) 2837–2845. doi:10.1111/j.1151-2916.1991.tb06852.x.
[33] Y. Swolfs, R.M. McMeeking, V.P. Rajan, F.W. Zok, I. Verpoest, L. Gorbatikh, Global load-sharing model for unidirectional hybrid fibre-reinforced composites, Journal of the Mechanics and Physics of Solids. 84 (2015) 380–394. doi:10.1016/j.jmps.2015.08.009.
[34] M. Ibnabdeljalil, W.A. Curtin, Strength and reliability of fiber-reinforced composites: Localized load-sharing and associated size effects, International Journal of Solids and Structures. 34 (1997) 2649–2668. doi:10.1016/S0020-7683(96)00179-5.
[35] J.G. Goree, R.S. Gross, Stresses in a three-dimensional unidirectional composite containing broken fibers, Engineering Fracture Mechanics. 13 (1980) 395–405. doi:10.1016/0013-7944(80)90068-5.
[36] S. Mahesh, I.J. Beyerlein, S.L. Phoenix, Size and heterogeneity effects on the strength of fibrous composites, Physica D: Nonlinear Phenomena. 133 (1999) 371–389. doi:10.1016/S0167-2789(99)00082-2.
[37] S. Mahesh, S.L. Phoenix, I.J. Beyerlein, Strength distributions and size effects for 2D and 3D composites with Weibull fibers in an elastic matrix, International Journal of Fracture. 115 (2002) 41–85. doi:10.1023/A:1015729607223.
[38] S.B. Batdorf, R. Ghaffarian, Size effect and strength variability of unidirectional composites, Int J Fract. 26 (1984) 113–123. doi:10.1007/BF01157548.
[39] S. Pimenta, S.T. Pinho, Hierarchical scaling law for the strength of composite fibre bundles, Journal of the Mechanics and Physics of Solids. 61 (2013) 1337–1356. doi:10.1016/j.jmps.2013.02.004.

[40] I.J. Beyerlein, C.M. Landis, Shear-lag model for failure simulations of unidirectional fiber composites including matrix stiffness, Mechanics of Materials. 31 (1999) 331–350. doi:10.1016/S0167-6636(98)00075-1.
[41] J.M. Guerrero, J.A. Mayugo, J. Costa, A. Turon, A 3D Progressive Failure Model for predicting pseudo-ductility in hybrid unidirectional composite materials under fibre tensile loading, Composites Part A: Applied Science and Manufacturing. 107 (2018) 579–591. doi:10.1016/j.compositesa.2018.02.005.
[42] S. Mahesh, S.L. Phoenix, Lifetime distributions for unidirectional fibrous composites under creep-rupture loading, International Journal of Fracture. 127 (2004) 303–360. doi:10.1023/B:FRAC.0000037675.72446.7c.
[43] A. Engelbrecht-Wiggans, S.L. Phoenix, A stochastic model based on fiber breakage and matrix creep for the stress-rupture failure of unidirectional continuous fiber composites, International Journal of Fracture. 217 (2019) 1–34. doi:10.1007/s10704-019-00359-9.
[44] T. Okabe, N. Takeda, Y. Kamoshida, M. Shimizu, W.A. Curtin, A 3D shear-lag model considering micro-damage and statistical strength prediction of unidirectional fiber-reinforced composites, Composites Science and Technology. 61 (2001) 1773–1787. doi:10.1016/S0266-3538(01)00079-3.
[45] R.P. Tavares, J.M. Guerrero, F. Otero, A. Turon, J.A. Mayugo, J. Costa, P.P. Camanho, Effects of local stress fields around broken fibres on the longitudinal failure of composite materials, International Journal of Solids and Structures. 156–157 (2019) 294–305. doi:10.1016/j.ijsolstr.2018.08.027.
[46] I.J. Beyerlein, S.L. Phoenix, A.M. Sastry, Comparison of shear-lag theory and continuum fracture mechanics for modeling fiber and matrix stresses in an elastic cracked composite lamina, International Journal of Solids and Structures. 33 (1996) 2543–2574. doi:10.1016/0020-7683(95)00172-7.
[47] S.L. Phoenix, I.J. Beyerlein, Statistical Strength Theory for Fibrous Composite Materials, in: Comprehensive Composite Materials, Elsevier, 2000: pp. 559–639. doi:10.1016/B0-08-042993-9/00056-5.
[48] D.R. King, T.L. Sun, Y. Huang, T. Kurokawa, T. Nonoyama, A.J. Crosby, J.P. Gong, Extremely tough composites from fabric reinforced polyampholyte hydrogels, Mater. Horiz. 2 (2015) 584–591. doi:10.1039/C5MH00127G.
[49] Y. Huang, D.R. King, T.L. Sun, T. Nonoyama, T. Kurokawa, T. Nakajima, J.P. Gong, Energy-Dissipative Matrices Enable Synergistic Toughening in Fiber Reinforced Soft Composites, Advanced Functional Materials. 27 (2017) 1605350. doi:10.1002/adfm.201605350.
[50] Z. Wang, C. Xiang, X. Yao, P. Le Floch, J. Mendez, Z. Suo, Stretchable materials of high toughness and low hysteresis, Proc Natl Acad Sci USA. 116 (2019) 5967–5972. doi:10.1073/pnas.1821420116.
[51] X. Feng, Z. Ma, J.V. MacArthur, C.J. Giuffre, A.F. Bastawros, W. Hong, A highly stretchable double-network composite, Soft Matter. 12 (2016) 8999–9006. doi:10.1039/C6SM01781A.
[52] F.T. Moutos, L.E. Freed, F. Guilak, A biomimetic three-dimensional woven composite scaffold for functional tissue engineering of cartilage, Nature Mater. 6 (2007) 162–167. doi:10.1038/nmat1822.
[53] S. Lin, C. Cao, Q. Wang, M. Gonzalez, J.E. Dolbow, X. Zhao, Design of stiff, tough and stretchy hydrogel composites via nanoscale hybrid crosslinking and macroscale fiber reinforcement, Soft Matter. 10 (2014) 7519–7527. doi:10.1039/C4SM01039F.
[54] I.-C. Liao, F.T. Moutos, B.T. Estes, X. Zhao, F. Guilak, Composite Three-Dimensional Woven Scaffolds with Interpenetrating Network Hydrogels to Create Functional Synthetic Articular Cartilage, Advanced Functional Materials. 23 (2013) 5833–5839. doi:10.1002/adfm.201300483.
[55] Y. Sha, C.Y. Hui, A. Ruina, E.J. Kramer, Continuum and Discrete Modeling of Craze Failure at a Crack Tip in a Glassy Polymer, Macromolecules. 28 (1995) 2450–2459. doi:10.1021/ma00111a044.
[56] B.D. Coleman, On the strength of classical fibres and fibre bundles, Journal of the Mechanics and Physics of Solids. 7 (1958) 60–70. doi:10.1016/0022-5096(58)90039-5.
[57] L. Mullins, Softening of Rubber by Deformation, Rubber Chemistry and Technology. 42 (1969) 339–362. doi:10.5254/1.3539210.
[58] R.E. Webber, C. Creton, H.R. Brown, J.P. Gong, Large Strain Hysteresis and Mullins Effect of Tough Double-Network Hydrogels, Macromolecules. 40 (2007) 2919–2927. doi:10.1021/ma062924y.
[59] Y. Mao, S. Lin, X. Zhao, L. Anand, A large deformation viscoelastic model for double-network hydrogels, Journal of the Mechanics and Physics of Solids. 100 (2017) 103–130. doi:10.1016/j.jmps.2016.12.011.

[60] H.M. Taylor, D.E. Sweitzer, On the current enhancement at the edge of a crack in a lattice of resistors, Advances in Applied Probability. 30 (1998) 342–364. doi:10.1239/aap/1035228073.
[61] T.A. Godfrey, J.N. Rossettos, S.E. Bosselman, The Onset of Tearing at Slits in Stressed Coated Plain Weave Fabrics, J. Appl. Mech. 71 (2004) 879. doi:10.1115/1.1794165.
[62] J.R. Rice, Mathematical analysis in the mechanics of fracture, Fracture: An Advanced Treatise. 2 (1968) 191–311.

Appendix: Solution of continuum model

We convert equations (11) and (12) into an anti-shear plane crack problem using the following transformations:

$$x_1 = X_1,\ x_2 = \alpha X_2,\ \tau_2 \equiv \frac{\sigma_{22}}{\alpha},\ \tau_1 \equiv \sigma_{12},\ \alpha = \sqrt{\frac{C_{22}}{C_{12}}}. \tag{A1}$$

The constitutive model, rewritten in the transformed stresses τ_2, τ_1 are isotropic, i.e.,

$$\begin{aligned} &\sigma_{22} = C_{22}\varepsilon_{22} = C_{22}\frac{\partial u_2}{\partial x_2} = \frac{C_{22}}{\alpha}\frac{\partial u_2}{\partial X_2} = \alpha\frac{C_{22}}{\alpha^2}\frac{\partial u_2}{\partial X_2} = \alpha C_{12}\frac{\partial u_2}{\partial X_2} \equiv \alpha\tau_2 \Rightarrow \tau_2 = C_{12}\frac{\partial u_2}{\partial X_2} \\ &\sigma_{12} = C_{12}\varepsilon_{12} \Rightarrow \sigma_{12} = \tau_1 = C_{12}\frac{\partial u_2}{\partial X_1} \end{aligned}. \tag{A2}$$

Further, τ_2, τ_1 satisfies equilibrium in the transformed plane (X_1, X_2)

$$\frac{\partial \sigma_{22}}{\partial x_2} + \frac{\partial \sigma_{12}}{\partial x_1} = 0 \Rightarrow \frac{\alpha\partial \tau_2}{\partial x_2} + \frac{\partial \tau_1}{\partial x_1} = 0 \Rightarrow \frac{\partial \tau_2}{\partial X_2} + \frac{\partial \tau_1}{\partial X_1} = 0. \tag{A3}$$

Equations (A2) and (A3) imply that u_2 is the displacement field of an anti-plane shear problem, and it satisfies the Laplace equation in the (X_1, X_2) plane

$$\frac{\partial^2 u_2}{\partial X_1^2} + \frac{\partial^2 u_2}{\partial X_2^2} = 0. \tag{A4}$$

Symmetry implies that we need to consider the upper half of the strip and the boundary conditions are:

$$u_2\left(|x_1| < \infty, x_2 = L\right) = \Delta, \quad \frac{\partial u_2}{\partial x_2}\left(-a < x < 0, x_2 = 0\right) = 0, \quad u_2\left(x_1 > 0, x_2 = 0\right) = u_2\left(x_1 < -a, x_2 = 0\right) = 0 \tag{A5}$$

Let $u_2 = \Delta\frac{x_2}{L} + u_2^* = \Delta\frac{X_2}{\bar{L}} + u_2^*$, where $\bar{L} = L/\alpha$. Note that stresses associated with $\Delta\frac{X_2}{\bar{L}}$ is $\sigma_{22} = C_{22}\Delta/L$ and $\sigma_{12} = 0$ everywhere in the strip. By equations (A3) and (A4), the displacement field u_2^* must satisfy Laplace equation in the (X_1, X_2) plane with boundary conditions

$$\begin{aligned} &u_2^*\left(|X_1| < \infty, X_2 = \bar{L}\right) = 0, \quad \frac{\partial u_2^*}{\partial X_2}\left(-a < X_1 < 0, X_2 = 0\right) = -\frac{\Delta}{\bar{L}}, \\ &u_2^*\left(X_1 > 0, X_2 = 0\right) = u_2^*\left(X_1 < -a, X_2 = 0\right) = 0 \end{aligned} \tag{A6}$$

Next, we map the strip in the (X_1, X_2) plane conformally onto the upper half η plane, where $\eta = \eta_1 + i\eta_2$. Let $z = X_1 + iX_2$, the conformal map is

$$\eta = \exp\left(\pi z / \bar{L}\right) \tag{A7}$$

The crack in the z plane maps onto $\eta \in \left(e^{-\pi a/\bar{L}}, 1\right)$ (the crack tips are mapped to $\eta = 1$ and $e^{-\pi a/\bar{L}}$ in the η plane). The top of the strip, $X_2 = \bar{L}$ is mapped onto the negative real η axis. This mapping transforms the displacement $u_2^*(X_1, X_2)$ onto a displacement $\hat{u}_2^*\left(\eta_1, \eta_2\right)$ in the η plane. Since the complex stress $\tau^*\left(z\right) = \tau_2^* + i\tau_1^*$ is analytic, the transformed stress $\hat{\tau}^*\left(\eta\right)$ in the η plane is also analytic and they are related by

$$\tau^* = \hat{\tau}^*\left(\eta\right)\frac{d\eta}{dz} = \frac{\pi}{\bar{L}}\eta\hat{\tau}^*\left(\eta\right) \tag{A8}$$

This means that the crack in the interval $\eta \in \left(e^{-\pi a/\bar{L}}, 1\right)$ is loaded by a negative traction $-C_{12}\dfrac{\Delta}{\bar{l}} \times \dfrac{\bar{l}}{\pi\eta}$. The complex stresses $\hat{\tau}^*\left(\eta\right)$ in the η plane can be found using a formula by Rice [62]:

$$\begin{aligned}\hat{\tau}^*\left(\eta\right) &= \frac{-C_{12}\Delta}{\pi^2\sqrt{\left(\eta-1\right)\left(\eta-e^{-\pi a/\bar{L}}\right)}}\int_{e^{-\pi a/\bar{L}}}^{1}\frac{\sqrt{\left(1-t\right)\left(t-e^{-\pi a/\bar{L}}\right)}}{t\left(t-\eta\right)}dt \\ &= -\frac{C_{12}\Delta}{\pi\eta} + \frac{C_{12}\Delta}{\pi\sqrt{\left(\eta-1\right)\left(\eta-e^{-\pi a/\bar{L}}\right)}}\left[\frac{\eta-\sqrt{e^{-\pi a/\bar{L}}}}{\eta}\right]\end{aligned} \tag{A9}$$

Using (A8), the stresses in the z plane is

$$\tau^*\left(z\right) = -\frac{C_{12}\Delta}{\bar{L}} + \frac{C_{12}\Delta\left[e^{\pi z/\bar{L}} - \sqrt{e^{-\pi a/\bar{L}}}\right]}{\bar{L}\sqrt{\left(e^{\pi z/\bar{L}}-1\right)\left(e^{\pi z/\bar{L}}-e^{-\pi a/\bar{L}}\right)}}. \tag{A10}$$

Equation (A10) is the stress associated with u_2^*, the stress associated with u_2 is

$$\tau\left(z\right) = \tau^*\left(z\right) + \frac{C_{12}\Delta}{\bar{L}} = \frac{C_{12}\Delta\left[e^{\pi z/\bar{L}} - \sqrt{e^{-\pi a/\bar{L}}}\right]}{\bar{L}\sqrt{\left(e^{\pi z/\bar{L}}-1\right)\left(e^{\pi z/\bar{L}}-e^{-\pi a/\bar{L}}\right)}} \tag{A11}$$

The actual stresses σ_{22} and σ_{12} can be obtained from (A11) using (A2), i.e., $\sigma_{22} = \alpha\tau_2, \sigma_{12} = \tau_1$ with $X_1 = x_1, X_2 = x_2/\alpha$. The case of $a \to \infty$ can be obtained by setting $a = \infty$ in (A11).